Journal of Power Sources 204 (2012) 53–59

Contents lists available at SciVerse ScienceDirect

Journal of Power Sources

journal homepage: www.elsevier.com/locate/jpowsour

Characterization of Ba-deficient $PrBa_{1-x}Co_2O_{5+\delta}$ as cathode material for intermediate temperature solid oxide fuel cells

Shengli Pang, Xuening Jiang*, Xiangnan Li, Qian Wang, Zhixian Su

Key Laboratory of Materials Modification by Laser, Ion and Electron Beams, Ministry of Education, Dalian University of Technology, Dalian 116024, People's Republic of China

ARTICLE INFO

Article history:
Received 7 November 2011
Received in revised form
26 December 2011
Accepted 1 January 2012
Available online 9 January 2012

Keywords:
Perovskite
Ba-deficiency
Cathode
Solid oxide fuel cell

ABSTRACT

A-site Ba-deficient $PrBa_{1-x}Co_2O_{5+\delta}$ ($PB_{1-x}CO$, $x = 0$–0.08) oxides are synthesized and evaluated as cathode materials for intermediate temperature solid oxide fuel cells (IT-SOFCs) with respect to crystal structure, chemical stability, thermal expansion behavior, electrical conduction and electrochemical performance. $PB_{1-x}CO$ with Ba-deficiency $x = 0$–0.08 has an orthorhombic structure, which shows lattice shrinkage with bigger x; higher Ba-deficiency $x = 0.1$ causes formation of impurity phases. The $PB_{1-x}CO$ oxides are chemically stable with $Gd_{0.1}Ce_{0.9}O_{1.95}$ (GDC) electrolyte at 1050 °C in air. Thermal expansion coefficient of $PB_{1-x}CO$ decreases slightly with higher Ba-deficiency. Electrical conductivity of $PB_{1-x}CO$ exhibits an initial decrease with higher Ba deficiency to $x = 0.03$ and then increases gradually to a maximum at $x = 0.08$. Introduction of Ba deficiency greatly improves electrochemical performance of $PB_{1-x}CO$, characterized by decreased area specific resistances (ASRs) with higher Ba deficiency. The ASR values as low as 0.115 Ω cm^2 and 0.093 Ω cm^2 have been obtained at 600 °C in air for $PB_{1-x}CO$ with $x = 0.05$ and 0.08 respectively. These results have demonstrated that the Ba-deficient $PB_{1-x}CO$ ($x = 0.03$–0.08) oxides are promising cathode materials for IT-SOFCs.

© 2012 Elsevier B.V. All rights reserved.

1. Introduction

Solid oxide fuel cells (SOFCs) are considered as promising energy conversion devices owing to their high working efficiency, low emissions and excellent fuel flexibility [1–3]. For the commercialization of SOFCs, one strategy being pursued for meeting the goals of cost reduction and enhanced durability is lowering the operating temperature to the intermediate temperature range of 600–800 °C [3–5]. The decrease in operating temperature, however, increases the cells' overpotential, and the main contributor to this increase is the cathode because of high activation energy of oxygen reduction reaction (ORR) [2,4]. Development of new cathode materials with high catalytic activity for ORR and low polarization resistances is therefore critical for intermediate temperature solid oxide fuel cells (IT-SOFCs).

In recent years, mixed ionic and electronic conducting (MIEC) $LnBaCo_2O_{5+\delta}$ (LnBCO, Ln = Lanthanide) oxides with double-layered perovskite structures have received increasing attention [4–17]. These LnBCO oxides have 112-type perovskite structures with alternating stacking layers of $[CoO_2]$–$[LnO_\delta]$–$[CoO_2]$–[BaO] along the c-axis and oxygen vacancies preferably located in the LnO_δ layer due to different radius of Ln^{3+} and Ba^{2+} ions and different Ba—O and Ln—O bond strength [4,6,7]. This A-site cation ordered perovskite structure was recognized to be able to greatly enhance the oxygen transport kinetics [8–10], the key factor that determines polarization resistance of the cathode [2], which then opens the possibility for developing a new class of materials suitable for SOFC cathodes.

Among the various LnBCO oxides, $PrBaCo_2O_{5+\delta}$ (PBCO) has been demonstrated to show the lowest area specific polarization resistances based on different electrolyte materials [5,11,13] due to its fast oxygen-ion diffusion and surface exchange kinetics [5,9–11]. The oxygen reduction mechanism of PBCO on $Sm_{0.2}Ce_{0.8}O_{1.9}$ (SDC) electrolyte was investigated by electrochemical impedance spectroscopy [15]. In order to further improve electrochemical performance of PBCO and decrease its thermal expansion coefficient (TEC), composition cathodes such as PBCO–GDC [9] and PBCO–SDC [5] as well as A-site or B-site cationic doping for PBCO [18–21] were studied. On the other hand, some researchers have found that A-site cationic deficiency introduced into the lattice structure of perovskite oxides significantly affects the physical and chemical properties of materials. Kostogloudis and Ftikos [22] and Zhou et al. [23] observed a gradual reduction in electrical conductivity and TEC with the increasing A-site cationic deficiency in $La_{0.6}Sr_{0.4-x}Co_{0.2}Fe_{0.8}O_{3-\delta}$ ($x = 0.0$–0.2) and $(Ba_{0.5}Sr_{0.5})_{1-x}Co_{0.8}Fe_{0.2}O_{3-\delta}$ ($x > 0$) respectively. Ge et al. [24] suggested that the reduced electronic conductivity could be attributed to the creation of additional oxygen vacancies, which was found to promote the process of oxygen ionic diffusion. Very recently, significantly improved electrochemical performance has been obtained for cationic deficient $Ba_{1-x}Co_{0.7}Fe_{0.2}Nb_{0.1}O_{3-\delta}$

* Corresponding author. Tel.: +86 41184708380x8204; fax: +86 41184708389.
E-mail address: xnjiang@dlut.edu.cn (X. Jiang).

0378-7753/$ – see front matter © 2012 Elsevier B.V. All rights reserved.
doi:10.1016/j.jpowsour.2012.01.034

(x = 0.00–0.15) oxides [26,27]. However, no work has been reported for cation-deficient PBCO oxide with respect to its performance as cathode material of SOFC.

In the present study, A-site Ba-deficient $PrBa_{1-x}Co_2O_{5+\delta}$ ($PB_{1-x}CO$, x = 0.00–0.08) oxides were synthesized and evaluated as cathode materials for IT-SOFCs. The effects of Ba deficiency on crystal structure, chemical stability with electrolyte materials, TEC, electrical conductivity, as well as electrochemical performance were studied. The experimental results have demonstrated that the A-site Ba-deficient $PB_{1-x}CO$ oxides are promising cathode materials for IT-SOFCs.

2. Experimental

2.1. Sample preparation

Double layered perovskite oxides $PB_{1-x}CO$ with Ba-deficiency x = 0, 0.03, 0.05, 0.08 and 0.1 were synthesized by a combined EDTA–citrate complexing sol–gel method. Briefly, $Pr(NO_3)_3{\cdot}6H_2O$ (AR), $Ba(NO_3)_2$ (AR) and $Co(NO_3)_3{\cdot}6H_2O$ (AR) at stoichiometric proportions of $PrB_{1-x}CO$ (x = 0.00–0.10) were firstly dissolved into EDTA–$NH_3{\cdot}H_2O$ solution (pH ≈ 6) to form an aqueous solution, and then acid–$NH_3{\cdot}H_2O$ solution (pH≈6) was added at a mole ratio of 1:1:2 for EDTA:total metal ions:citric acid. The mixed solution was heated at 80 °C and 150 °C in sequence to obtain a dark dry foam structure. The precursor was decomposed on a hot plate, followed by calcination at 1050 °C for 12 h in air to yield the desired powders. The as-synthesized $PB_{1-x}CO$ powders were mixed with $Ce_{0.9}Gd_{0.1}O_{1.95}$ (GDC) electrolyte in a 50/50 weight ratio followed by calcination at 1050 °C for 4 h in air for study of their chemical compatibility.

2.2. Characterization

Phase structures of the as-synthesized $PB_{1-x}CO$ powders and the calcined $PB_{1-x}CO$–GDC mixed powders were characterized by X-ray diffraction measurement (XRD, Rigaku D/Max 2400). The XRD patterns were collected at room temperature with step size of 0.02° in 2θ over the scanning angular range of 20°–80°. Thermal expansion data of $PB_{1-x}CO$ were collected with a dilatometer (Netzsch DIL 402PC) in the temperature range of 30–900 °C in air with a heating rate of 5 °C min^{-1}. The electrical conductivities of $PB_{1-x}CO$ (x = 0.00–0.08) were measured at various temperatures in air by a DC four-electrode method using Au paste as electrodes. Symmetrical cells with the configuration of $PB_{1-x}CO$/GDC/$PB_{1-x}CO$ were applied for electrochemical impedance study. Dense GDC pellets with a diameter of ~10 mm and thickness of ~1 mm were obtained by pressing followed by calcination at 1350 °C for 7 h in air. The $PB_{1-x}CO$ ink (prepared by mixing the cathode powders with α-terpineol and ethyl cellulose) was then screen-printed onto both sides of the GDC pellet, which was calcined at 1050 °C for 2 h in air. The obtained symmetrical cell was spring-loaded onto a home-made sample holder. Fine (100-mesh) gold gauzes were slightly pressed on both sides of the cell as current collectors. The impedance measurements were conducted using a Solartron 1260 Frequency Response Analyzer combined with a Solartron 1287 potentiostat under open circuit voltage (OCV) condition in the frequency range of 10^{-1}–10^5 Hz, and at temperatures of 600–800 °C in air with intervals of 50 °C.

3. Results and discussion

3.1. Phase structure and chemical stability

Fig. 1 presents XRD patterns of the $PB_{1-x}CO$ (x = 0.00–0.10) powders after fired at 1050 °C for 12 h in air. It is observed that pure

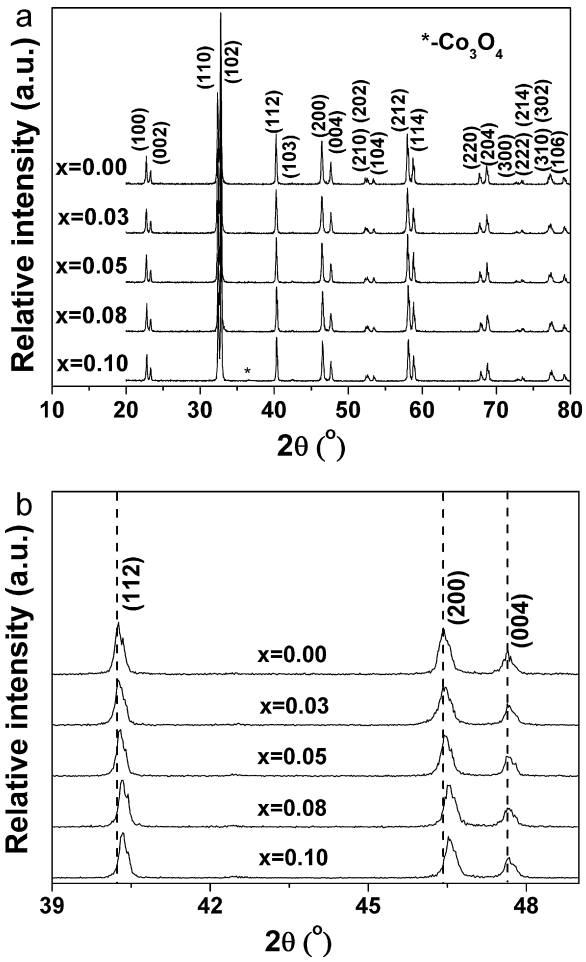

Fig. 1. The whole (a) and magnified (b) XRD patterns of $PB_{1-x}CO$ (x = 0.00–0.10) oxides calcined at 1050 °C for 12 h in air.

phases with an orthorhombic perovskite structure were obtained for the $PB_{1-x}CO$ oxides with Ba-deficiency x = 0.00–0.08, while impurity of Co_3O_4 was found for the sample with x = 0.1. This suggests that the A-site Ba-deficiency fraction (x) was limited to approximately 0.08 for $PB_{1-x}CO$ oxide. As depicted in Fig. 1b, the (1 1 2) diffraction peak gradually shifts to higher 2θ angle with the increasing Ba-deficiency, indicating a shrinkage in the perovskite lattice. Additionally, the (2 0 0) diffraction peaks shifts likewise while the (0 0 4) peaks remains almost unchanged in position, which demonstrates that the structural shrinkage in $PB_{1-x}CO$ caused by Ba-deficiency is mainly along a and/or b directions.

Chemical compatibility between component materials is necessary for long-term stability of SOFCs. The chemical reactivity of $PB_{1-x}CO$ (x = 0.00–0.08) with GDC electrolyte was studied by firing the $PB_{1-x}CO$–GDC mixed powders (in 1:1 weight ratio) at 1050 °C for 4 h in air. The XRD results of the calcined mixed powders (Fig. 2) show that no additional phase was formed and no obvious XRD peak shift could be observed for each sample. Thus the Ba-deficient $PB_{1-x}CO$ (x = 0.00–0.08) oxides are chemically stable cathode materials for SOFCs using GDC as electrolyte.

3.2. Thermal expansion behavior

Thermal expansion curves of the $PB_{1-x}CO$ (x = 0.00–0.08) samples measured in air are presented in Fig. 3. The calculated thermal expansion coefficients (TECs) in three different temperature ranges are listed in Table 1. The results show that the TEC of $PB_{1-x}CO$ is highly dependent upon the selected temperature range while

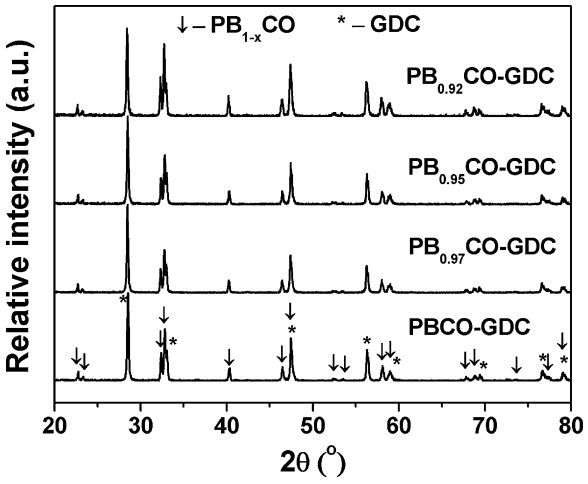

Fig. 2. XRD patterns of the $PB_{1-x}CO$–GDC mixed powders calcined at 1050 °C for 4 h in air.

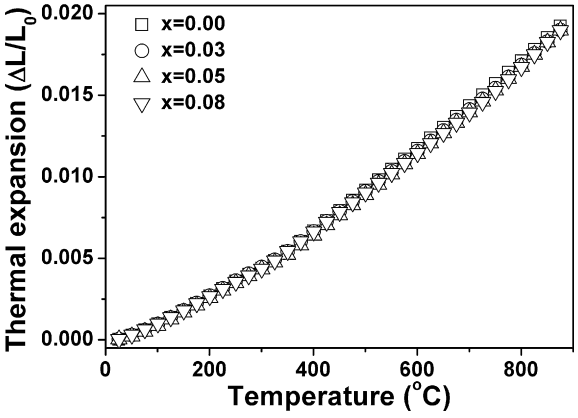

Fig. 3. Thermal expansion curves of $PB_{1-x}CO$ (x = 0.00–0.08) measured in air.

slightly upon the A-site Ba-deficiency. The apparent thermal expansion behavior for the mixed conducting perovskite oxides can be ascribed to crystal expansion from anharmonic atomic vibrations dependent on the electrostatic attraction forces within the lattice, and to chemical expansion induced by both the cobalt ion spin transition and reduction of cobalt ions to lower oxidation states [23,27]. As evidenced in $PrBaCo_2O_{5+\delta}$ [9], the inflections of the thermal expansion curves of $PB_{1-x}CO$ oxides at around 300 °C (Fig. 2) were associated with reduction of Co^{4+} to Co^{3+} ions caused by thermal-driven releasing of lattice oxygen. This chemical expansion contributes to the higher TEC values for the temperature range of 300–900 °C than for the temperature range below 300 °C (Table 1). On the other hand, higher Ba-deficiency led to a slight decrease in TEC for the $PB_{1-x}CO$ oxides. Increased electrostatic attraction resulting from shrinkage of the perovskite structure (Fig. 1) may be responsible for this phenomenon [23,27]. The smallest TEC value is 22.8×10^{-6} °C^{-1} at 30–900 °C for $PB_{1-x}CO$ with

Table 1
Thermal expansion coefficients (TECs) of $PB_{1-x}CO$ oxides at various temperature ranges.

x	TEC × 10^{-6} (°C^{-1})		
	30–300 °C	300–900 °C	30–900 °C
0.00	16.7	26.1	23.4
0.03	17.0	25.5	23.0
0.05	16.6	25.8	23.0
0.08	16.3	25.4	22.8

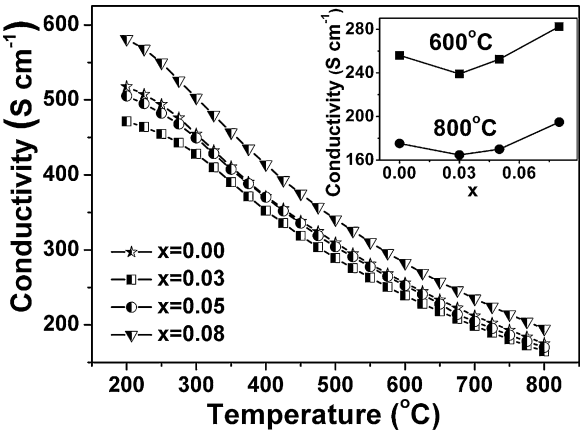

Fig. 4. Temperature-dependence of electrical conductivity of $PB_{1-x}CO$ (x = 0.00–0.08) oxides in air.

x = 0.08, which, however, is still much larger than TEC of the commonly used intermediate temperature electrolytes of GDC [28], $La_{0.9}Sr_{0.1}Ga_{0.8}Mg_{0.2}O_{2.85}$ (LSGM) [4] and $Sm_{0.2}Ce_{0.8}O_{1.9}$ (SDC) [29]. In order to further reduce TEC of the $PB_{1-x}CO$ oxides and improve structural compatibility between the cathode and electrolyte materials, future work will be focused on composite cathode or partial substitution of B-site Co ions with more stable ions such as Fe, Cu, Mo and Nb [20,21,27,30].

3.3. Electrical conductivity

Fig. 4 presents electrical conductivity of $PB_{1-x}CO$ (x = 0.00–0.08) oxides as a function of temperature (200–800 °C) in air. The conductivity decreases with higher temperature demonstrating a metal-like behavior. The values of conductivity in the measured temperature range are above 130 S cm^{-1} for all the samples, which meet the requirement of a SOFC cathode material regarding the conductivity (>100 S cm^{-1}) [20]. Furthermore, as shown in the insert, across all values of x examined, the electrical conductivity of $PB_{1-x}CO$ oxides exhibits an initial decrease with increasing Ba deficiency (from x = 0.00 to x = 0.03) and then increases gradually to a maximum at x = 0.08. Different trends of conductivity were reported in other A-site cation deficient perovskite oxides. Both Zhou et al. [23] and Kostogloudis and Ftikos [22] observed a gradual decrease in conductivity with higher cationic deficiency for the oxides of $(Ba_{0.5}Sr_{0.5})_{1-x}Co_{0.8}Fe_{0.2}O_{3-\delta}$ (x = 0–0.15) and $La_{0.6}Sr_{0.4-x}Co_{0.2}Fe_{0.8}O_{3-\delta}$ (x = 0–0.2) respectively. They ascribed such conductive behaviors to generation of additional oxygen vacancies with increasing A-site cationic deficiency, which could perturb the O–Co–O periodic potential, result in carrier localization and thus caused decrease in conductivity [5,23]. On the contrary, Yang et al. [27] found a gradual increase in conductivity with increasing Ba deficiency in $Ba_{1-x}Co_{0.7}Fe_{0.2}Nb_{0.1}O_{3-\delta}$ (x = 0.00–0.15) oxides, and deduced that oxidation of B-site ions to a higher valence should be responsible for this phenomenon. Generally, conductive behavior in the cobalt-based perovskite oxides (p-type conductors) is closely related to concentration of the tetravalent cobalt ions (Co^{4+}), which are charge carriers of the electrons, and generation of oxygen vacancies ($V_O^{\bullet\bullet}$) which can inhibit the electronic conduction. According to defect chemistry, the negative charges introduced by Ba^{2+} substitution for Pr^{3+} at A-sites of PBCO are compensated by both generation of oxygen vacancy and oxidation of B-site Co^{3+} ions to Co^{4+} [31], which play an opposite role for the electrical conductivity. The additional negative charges introduced by A-site Ba-deficiency, 2× per one $PB_{1-x}CO$ molecule, are to be compensated likewise. If compensation for the negative

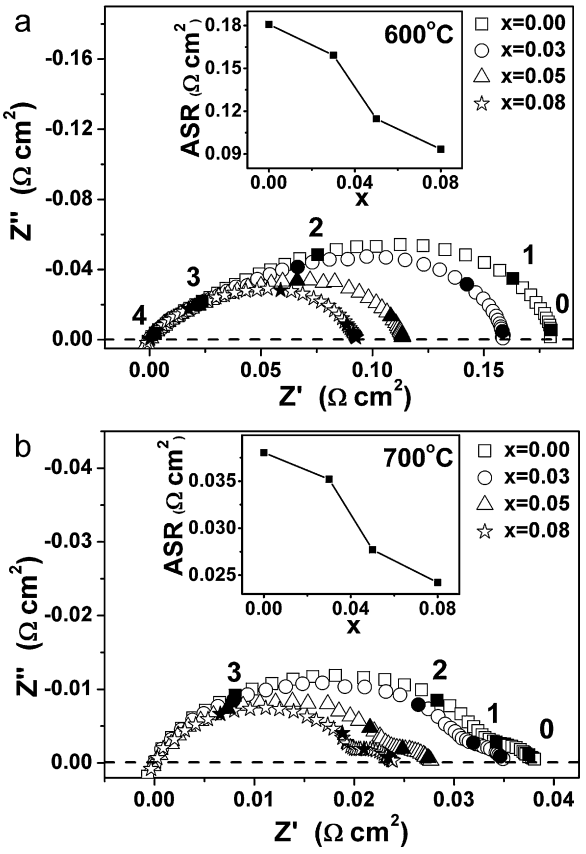

Fig. 5. Electrochemical impedance spectra and area specific resistances (ASRs) of $PB_{1-x}CO$ (x = 0.00–0.08) cathodes at (a) 600 °C and (b) 700 °C in air. The numbers in these plots correspond to logarithm of frequency.

charges (2×) is dominated by generation of oxygen vacancy, the conductivity will decrease with higher Ba-deficiency, like the cases of $(Ba_{0.5}Sr_{0.5})_{1-x}Co_{0.8}Fe_{0.2}O_{3-\delta}$ [23] and $La_{0.6}Sr_{0.4-x}Co_{0.2}Fe_{0.8}O_{3-\delta}$ [22]; while when oxidation of cobalt ions dominates the charge compensation, the conductivity will increase with higher Ba-deficiency, like the $Ba_{1-x}Co_{0.7}Fe_{0.2}Nb_{0.1}O_{3-\delta}$ oxide [27]. Therefore, the conductivity transition of $PB_{1-x}CO$ at Ba-deficiency x = 0.03 as shown in the insert of Fig. 4 might be associated with a change in dominant charge compensation mechanism.

3.4. Electrochemical performance

The electrochemical performance of $PB_{1-x}CO$ (x = 0.00–0.08) was characterized on the GDC electrolyte in a symmetrical cell configuration of $PB_{1-x}CO$/GDC/$PB_{1-x}CO$. Typical impedance spectra are given in Fig. 5. The ohmic resistances (intercepts at the high frequency with the real axis) arising from the GDC electrolyte and lead wires were normalized to zero for clarity. The area specific resistances (ASR), corresponding to the difference between the intercepts with the real axis at high and low frequency, are inserted in Fig. 5 as a function of Ba deficiency. It was found that increase of Ba deficiency resulted in a significant decrease in ASR of $PB_{1-x}CO$. Typically, the ASR value at 600 °C decreased ~50% when the Ba deficiency increased from x = 0.00 (ASR = 0.181 Ω cm²) to x = 0.08 (ASR = 0.093 Ω cm²). These results demonstrated that introduction of A-site Ba-deficiency effectively improved electrochemical performance of PBCO. A-site cationic deficiency in perovskite oxides was found to induce the preferential formation of oxygen vacancies for charge compensation [22,24]. As reviewed by Adler [2], high concentration of oxygen vacancy promotes the processes of oxygen surface exchange as well as oxygen ionic bulk transport,

Table 2
Area specific resistances (ASRs) of $PB_{1-x}CO$ (x = 0.00–0.08) cathodes measured at various temperatures in air.

x	ASR (Ω cm²)				
	600 °C	650 °C	700 °C	750 °C	800 °C
0.00	0.181	0.080	0.038	0.020	0.009
0.03	0.159	0.075	0.035	0.018	0.008
0.05	0.115	0.054	0.028	0.015	0.008
0.08	0.093	0.045	0.024	0.012	0.007

which were found experimentally [9,25,26] to result in the low polarization resistances of the cathodes. Distribution of the oxygen vacancies also influences oxygen surface reactivity and ionic bulk diffusion (ionic conduction) of the perovskite-typed cathodes [7–9]. In the A-site cationic ordered LnBCO perovskite oxides, oxygen vacancies are preferably located in the LnO_δ layer, thus the oxygen diffusion is restricted within the LnO_δ plane [4,6,7,11]. In the case of $PB_{1-x}CO$ oxides, deficiency of Ba^{2+} ions was expected to generate oxygen vacancies, if there are any, preferably on the BaO layers due to break of the Ba—O bonds. Thus, the anisotropic ionic diffusion on the PrO_δ planes of the PBCO oxide [11] was broken and three-dimensional oxygen ionic diffusion with shortened ionic diffusion path could be realized, which probably also contributed to the decreased polarization resistance of Ba-deficient $PB_{1-x}CO$ than the parent PBCO oxide [7,11].

The ASRs of $PB_{1-x}CO$ (x = 0.00–0.08) cathodes are listed in Table 2 and plotted as a function of temperature in Fig. 6. As expected, the ASR decreases significantly with higher temperature and Ba deficiency. Among the samples, the $PB_{0.92}CO$ oxide with Ba-deficiency x = 0.08 showed the best electrochemical performance with ASR value ranging from 0.093 Ω cm² at 600 °C to 0.007 Ω cm² at 800 °C in air. These values are much lower than the reported cationic-stoichiometric PBCO-related cathodes [5,9,11,13,15,18–21] and are comparable, if not higher, with those of other perovskite cathodes such as $Ba_{0.5}Sr_{0.5}Co_{0.8}Fe_{0.2}O_{3-\delta}$ [32] (0.172 Ω cm² at 600 °C and 0.042 Ω cm² at 700 °C) and $BaCo_{0.7}Fe_{0.3-y}Nb_yO_{3-\delta}$ [3] (0.13 Ω cm² at 600 °C and 0.0082 Ω cm² at 800 °C). Even the sample with a small Ba-deficiency x = 0.03, $PB_{0.97}CO$, exhibited a low ASR value of 0.159 Ω cm² at 600 °C. These results demonstrated the potential applications of these Ba-deficient $PB_{1-x}CO$ (x = 0.03–0.08) oxides as cathode materials for IT-SOFCs. What is more, the activation energy for the polarization resistance was found to decrease gradually with the increasing Ba deficiency in the $PB_{1-x}CO$ oxides, which suggested that introduction of the Ba-deficiency could facilitate the electrode reaction over the $PB_{1-x}CO$ cathodes.

To get further knowledge of effects of Ba deficiency on the electrochemical performance of PBCO, the impedance spectra were

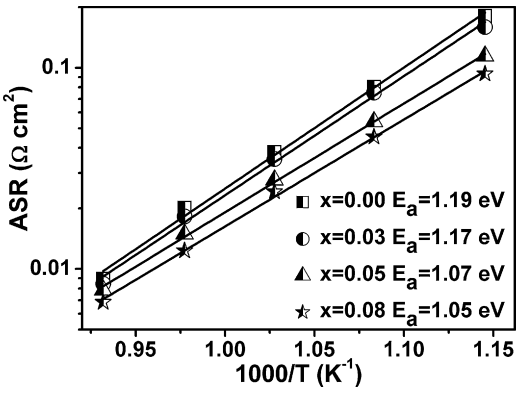

Fig. 6. Temperature-dependence of ASR for $PB_{1-x}CO$ (x = 0.00–0.08) cathodes measured in air. The corresponding activation energy (E_a) is given.

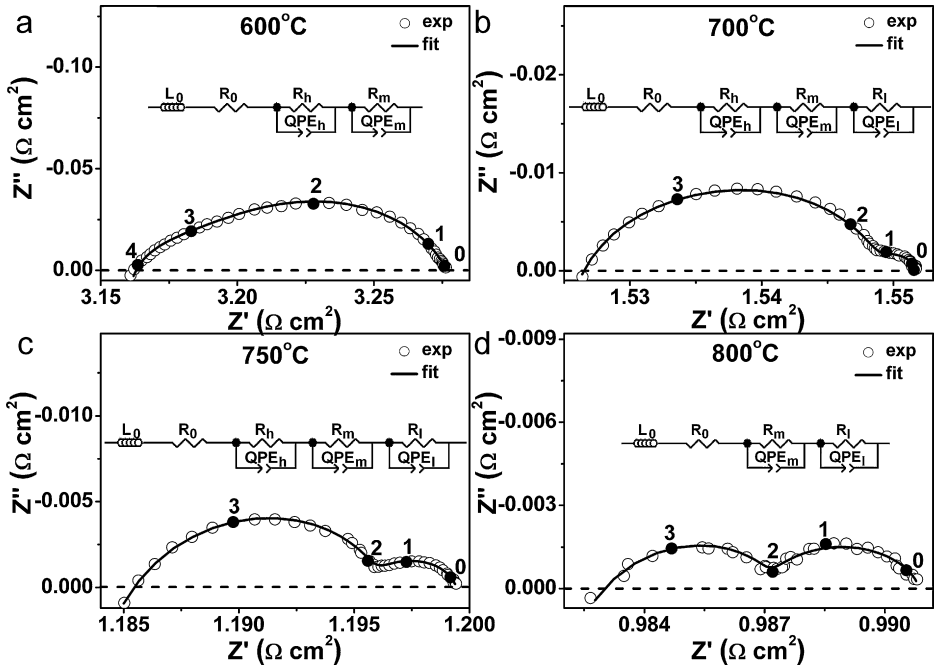

Fig. 7. Experimental and fitting results of impedance spectra for the $PB_{0.95}CO/GDC/PB_{0.95}CO$ symmetrical cell measured at various temperatures in air. The adopted equivalent circuit models are presented in each plot. The numbers in these plots correspond to logarithm of frequency.

fitted by the Zview software using equivalent circuit models. As a typical example, the impedance spectra of $PB_{0.95}CO$ ($x = 0.05$) measured at various temperatures in air are shown in Fig. 7 together with the adopted equivalent circuit models and fitting curves. The corresponding fitting results are given in Table 3. In these equivalent circuit models, L_0 is inductance originating from equipment and connection cables; R_0 is ohmic resistance mainly arising from the GDC electrolyte and lead wires; the components, (R_hQPE$_h$), (R_mQPE$_m$) and (R_lQPE$_l$), in series represent reaction step in high-frequency (HF), medium-frequency (MF) and low-frequency (LF) range respectively. Three depressed arcs at high, medium and low frequencies were identified in the whole temperature range, indicating at least three distinguishable processes taking place over the electrode. The HF (>10^3 Hz) and MF (10^3–10 Hz) arcs were overlapped as a depressed semi-circle and showed a significant decrease with increasing temperature; an additional LF arc (<10^2 Hz) was identified at the temperatures of 700 °C and above. With the fitting results shown in Table 3, the characteristic capacitance (C_i) and angular relaxation frequency (f_i), which are useful parameters in identifying the sub-steps of cathode reaction, were calculated based on the following equations [33] and also listed in Table 3:

$$C_i = \frac{(R_i Q_i)^{1/n_i}}{R_i} \quad (1)$$

$$f_i = \frac{(R_i Q_i)^{-1/n_i}}{2\pi} \quad (2)$$

The impedance spectra of other $PB_{1-x}CO$ ($x = 0$, 0.03, 0.08) samples were fitted likewise. The obtained resistances of R_h, R_m and R_l associated with the respective HF, MF and LF process for the $PB_{1-x}CO$ ($x = 0$, 0.03, 0.05 and 0.08) cathodes were plotted as a function of temperature in Fig. 8a, b and c respectively. The calculated activation energy (E_a) associated with specific process was also listed. The activation energy for the HF arcs (Fig. 8a) ranges from 1.24 eV to 1.38 eV and the corresponding relaxation frequency and capacitance are 10^3–10^5 Hz and 10^{-5}–10^{-3} F cm^{-2} respectively, which

Table 3
The fitting parameters for the impedance spectra (Fig. 7) of $PB_{0.95}CO/GDC/PB_{0.95}CO$ symmetric cell measured at various temperatures in air.

	T (°C)	600	650	700	750	800
	L_0 (H)	8.02×10^{-7}	1.02×10^{-6}	1.19×10^{-6}	1.167×10^{-6}	1.13×10^{-6}
	R_0 (Ω cm^2)	2.62	1.78	1.31	1.03	0.86
Arc$_h$	R_h (Ω cm^2)	4.72×10^{-2}	1.92×10^{-2}	8.43×10^{-3}	3.82×10^{-3}	–
	QPE$_h$-Q (F cm^{-2})	9.21×10^{-3}	1.12×10^{-2}	1.25×10^{-2}	1.65×10^{-2}	–
	QPE$_h$-n	0.57	0.77	0.89	1.01	–
	C_h (F cm^{-2})	2.72×10^{-5}	9.19×10^{-4}	3.84×10^{-3}	1.83×10^{-2}	–
	F_h (Hz)	1.24×10^{5}	9.02×10^{3}	4.92×10^{3}	2.27×10^{3}	–
Arc$_m$	R_m (Ω cm^2)	5.29×10^{-2}	2.58×10^{-2}	1.38×10^{-2}	7.07×10^{-3}	5.42×10^{-3}
	QPE$_m$-Q (F cm^{-2})	3.36×10^{-2}	3.57×10^{-2}	3.32×10^{-2}	4.06×10^{-2}	2.92×10^{-2}
	QPE$_m$-n	0.86	0.90	0.92	0.94	0.92
	C_m (F cm^{-2})	1.20×10^{-2}	1.61×10^{-2}	1.67×10^{-2}	2.38×10^{-2}	1.33×10^{-2}
	F_m (Hz)	2.50×10^{2}	3.82×10^{2}	6.88×10^{2}	9.45×10^{2}	2.20×10^{3}
Arc$_l$	R_l (Ω cm^2)	–	3.31×10^{-3}	4.09×10^{-3}	3.49×10^{-3}	3.76×10^{-3}
	QPE$_l$-Q (F cm^{-2})	–	16.55	13.72	12.77	12.91
	QPE$_l$-n	–	0.88	0.84	0.89	0.86
	C_l (F cm^{-2})	–	11.31	7.78	8.80	7.85
	F_l (Hz)	–	4.26	5.00	5.18	5.39

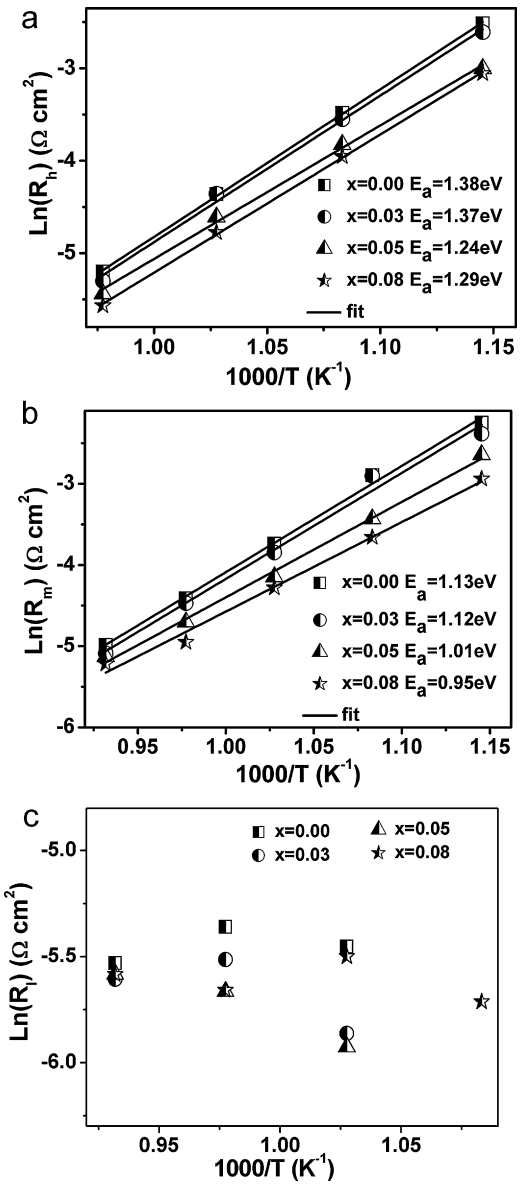

Fig. 8. Arrhenius plots and activation energies (E_a) of the resistances (a) R_h, (b) R_m and (c) R_l associated with the respective HF, MF and LF process for the $PB_{1-x}CO/GDC/PB_{1-x}CO$ ($x = 0$, 0.03, 0.05 and 0.08) symmetric cell measured in air.

are consistent with the characteristics associated with the oxygen ion diffusion through the cathode followed by a charge transfer at the electrode/electrolyte interface [15,34–36]. The MF arcs are characterized by the relaxation frequency of 10^2–10^3 Hz, capacitance of 6.2×10^{-3} to 2.5×10^{-2} F cm^{-2}, and activation energy of 0.95–1.13 eV (Fig. 8b), which are typical values for the electrode reaction process possibly rate-determined by electronic charge transfer at the surface of the electrode involving atomic oxygen, according to the reported results [15,23,37]. Especially large capacitances, 6–13 F cm^{-2}, were obtained for the LF arcs. Such large capacitance values are unlikely to be from any electrochemical process and are generally assigned to gas phase diffusion process through the porous cathode [15,35,38,39]. Adler [2] addressed origination and features of the gas-phase effect on the impedance spectra results of the porous SOFC cathodes in a review of "Factors Governing Oxygen Reduction in Solid Oxide Fuel Cell Cathodes". He proposed, based on a summary of many reported results that the resistance from the gas-phase diffusion is associated with various factors such as diffusion coefficient of oxygen in air, microstructures and thickness of the cathode, temperature as well as oxygen partial pressure. As depicted in Fig. 8a and b, increasing Ba deficiency in the $PB_{1-x}CO$ oxide effectively decreased the polarization resistances R_h and R_m resulting from the HF and MF process respectively. The associated activation energy also experienced a gradual decrease with higher Ba deficiency except for the R_h of $PB_{0.92}CO$. In contrast, polarization resistance associated with the LF process (Fig. 8c) showed little dependence on the Ba deficiency. Thus, we generally concluded that introduction of Ba deficiency to the double-layered perovskite oxide PBCO significantly enhanced the electrode reaction process (MF process) and the process of oxygen ion bulk diffusion followed by a charge transfer at the electrode/electrolyte interface (HF process), while hardly influenced the low-frequency gas phase diffusion process.

4. Conclusions

The effect of A-site Ba-deficiency on crystal structure, thermal expansion behavior, electrical conductivity and electrochemical performance of double-layered perovskite oxides $PrBa_{1-x}Co_2O_{5+\delta}$ ($PB_{1-x}CO$, $x = 0.00$–0.08) have been studied. The Ba-deficiency concentration in $PB_{1-x}CO$ was limited up to $x = 0.08$. No reaction between $PB_{1-x}CO$ and GDC electrolyte was found at 1050 °C in air. A slight decrease in thermal expansion coefficient was obtained with the increasing Ba deficiency. The electrical conductivity of $PB_{1-x}CO$ oxides exhibits an initial decrease with higher Ba deficiency to $x = 0.03$ and then increases gradually to a maximum at $x = 0.08$, which suggests a change in dominant charge compensation mechanism. Introduction of Ba deficiency was found to greatly improve electrochemical performance of $PB_{1-x}CO$, characterized by decreased area specific resistances (ASRs) with higher Ba deficiency. These experimental results have demonstrated that the Ba-deficient $PB_{1-x}CO$ ($x = 0.03$–0.08) oxides are potential cathode materials for IT-SOFCs.

Acknowledgements

This work was financially supported by the Scientific Research Foundation for the Returned Overseas Chinese Scholars, State Education Ministry.

References

[1] B.C.H. Steele, A. Heinzel, Nature 414 (2001) 345–352.
[2] S.B. Adler, Chem. Rev. 104 (2004) 4791–4843.
[3] C.J. Zhu, X.M. Liu, C.S. Yi, L. Pei, D.T. Yan, J.P. Niu, D.J. Wang, W.H. Su, Electrochem. Commun. 11 (2009) 958–961.
[4] J.-H. Kim, A. Manthiram, J. Electrochem. Soc. 155 (4) (2008) B385–B390.
[5] Q.J. Zhou, F. Wang, Y. Shen, T.M. He, J. Power Sources 195 (2010) 2174–2181.
[6] C. Frontera, A. Caneiro, A.E. Carrillo, J. Oró-Solé, J.L. García-Muñoz, Chem. Mater. 17 (2005) 5439–5445.
[7] J.-H. Kim, L. Mogni, F. Prado, A. Caneiro, J.A. Alonso, A. Manthiram, J. Electrochem. Soc. 156 (12) (2009) B1376–B1382.
[8] A.A. Taskin, A.N. Lavrov, Y. Ando, Appl. Phys. Lett. 86 (2005), 091910-1-3.
[9] G. Kim, S. Wang, A.J. Jacobson, L. Reimus, P. Brodersen, C.A. Mims, J. Mater. Chem. 17 (2007) 2500–2505.
[10] G. Kim, S. Wang, A.J. Jacobson, Z. Yuan, W. Donner, C.L. Chen, L. Reimus, P. Brodersen, C.A. Mims, Appl. Phys. Lett. 88 (2006), 024103-1-3.
[11] K. Zhang, L. Ge, R. Ran, Z.P. Shao, S.M. Liu, Acta Mater. 56 (2008) 4876–4889.
[12] S.L. Pang, X.N. Jiang, X.N. Li, Q. Wang, Q.Y. Zhang, Mater. Chem. Phys. 131 (2012) 642–646.
[13] E. Chavez, M. Mueller, L. Mogni, A. Caneiro, J. Phys.: Conf. Ser. 167 (2009), 012043-1-6.
[14] C.J. Zhu, X.M. Liu, C.S. Yi, D.T. Yan, W.H. Su, J. Power Sources 185 (2008) 193–196.
[15] D.J. Chen, R. Ran, K. Zhang, J. Wang, Z.P. Shao, J. Power Sources 188 (2009) 96–105.
[16] A. Tarancón, M. Burriel, J. Santiso, S.J. Skinner, J.A. Kilner, J. Mater. Chem. 20 (2010) 3799–3813.
[17] A.J. Jacobson, Chem. Mater. 22 (2010) 660–674.
[18] H.P. Ding, X.J. Xue, Electrochim. Acta 55 (2010) 3812–3816.
[19] J.H. Kim, M. Cassidy, J.T.S. Irvine, J. Bae, J. Electrochem. Soc. 156 (6) (2009) B682–B689.

[20] L. Zhao, Q. Nian, B.B. He, B. Lin, H.P. Ding, S.L. Wang, R.R. Peng, G.Y. Meng, X.Q. Liu, J. Power Sources 195 (2010) 453–456.
[21] L. Zhao, J.C. Shen, B.B. He, F.L. Chen, C.R. Xia, Int. J. Hydrogen Energy 36 (2011) 3658–3665.
[22] G.Ch. Kostogloudis, Ch. Ftikos, Solid State Ionics 126 (1999) 143–151.
[23] W. Zhou, R. Ran, Z.P. Shao, W.Q. Jin, N.P. Xu, J. Power Sources 182 (2008) 24–31.
[24] L. Ge, W. Zhou, R. Ran, S.M. Liu, Z.P. Shao, W.Q. Jin, N.P. Xu, J. Membr. Sci. 306 (2007) 318–328.
[25] Z.P. Shao, S.M. Haile, Nature 431 (2004) 170–173.
[26] Z. Liu, L.Z. Cheng, M.F. Han, J. Power Sources 196 (2011) 868–871.
[27] Z.B. Yang, M.F. Han, P.Y. Zhu, F. Zhao, F.L. Chen, Int. J. Hydrogen Energy 36 (2011) 9162–9168.
[28] H. Hayashi, M. Kanoh, C.J. Quan, H. Inaba, S.R. Wang, M. Dokiya, H. Tagawa, Solid State Ionics 132 (2000) 227–233.
[29] E.Yu. Pikalova, V.I. Maragou, A.N. Demina, A.K. Demin, P.E. Tsiakaras, J. Power Sources 181 (2008) 199–206.
[30] T. Nagai, W. Ito, T. Sakon, Solid State Ionics 177 (2007) 3433–3444.
[31] J.W. Stevenson, T.R. Armstrong, R.D. Carneim, L.R. Pederson, W.J. Weber, J. Electrochem. Soc. 143 (9) (1996) 2722–2729.
[32] R. Su, Z. Lü, K.F. Chen, N. Ai, S.Y. Li, B. Wei, W.H. Su, Electrochem. Commun. 10 (2008) 844–847.
[33] M.J. Escudero, A. Aguadero, J.A. Alonso, L. Daza, J. Electroanal. Chem. 611 (2007) 107–116.
[34] J. Peña-Martínez, D. Marrero-López, J.C. Ruiz-Morales, P. Núñez, C. Sánchez-Bautista, A.J.Dos. Santos-García, J. Canales-Vázquez, Int. J. Hydrogen Energy 34 (2009) 9486–9495.
[35] S.B. Adler, J.A. Lane, B.C.H. Steele, J. Electrochem. Soc. 143 (11) (1996) 3554–3564.
[36] F.S. Baumann, J. Fleig, H.-U. Habermeier, J. Maier, Solid State Ionics 177 (2006) 3187–3191.
[37] R. Barfod, M. Mogensen, T. Klemensø, A. Hagen, Y.L. Liu, P.V. Hendriksen, J. Electrochem. Soc. 154 (4) (2007) B371–B378.
[38] V.Ch. Kournoutis, F. Tietz, S. Bebelis, Fuel Cells 09 (6) (2009) 852–860.
[39] X.N. Li, X.N. Jiang, S.L. Pang, Q. Wang, Z.X. Su, Q.Y. Zhang, Int. J. Hydrogen Energy 36 (2011) 13850–13857.